Translational Oncology
www.transonc.com

Volume 11 Number xx Month 2017 pp. 1–10 1

Distinct Ezrin Truncations Differentiate Metastases in Sentinel Lymph Nodes from Unaffected Lymph Node Tissues, from Primary Breast Tumors, and from Healthy Glandular Breast Tissues

Claudia Röwer[*,1], Christian George[*,†,1], Toralf Reimer[†], Bernd Stengel[‡], Anngret Radtke[‡,2], Bernd Gerber[†] and Michael O. Glocker[*]

[*]Proteome Center Rostock, University of Rostock, Schillingallee 69, 18057 Rostock, Germany; [†]Department of Obstetrics and Gynecology, University of Rostock, Südring 81, 18059 Rostock, Germany; [‡]Partnerschaft der Fachärzte für Pathologie, Südstadt Clinical Center, Südring 81, 18059 Rostock, Germany

Abstract

BACKGROUND: Lymph node metastasis status is a prognostic factor for further lymph node involvement and for patient survival in breast cancer patients. Frozen section analysis of lymph nodes is a reliable method for detection of macro-metastases. However, this method is far less effective in detecting micro-metastases, requesting improved diagnostic procedures. METHODS: We investigated expression and truncation of ezrin in (i) sentinel lymph node metastases, (ii) unaffected axillary lymph nodes, (iii) primary breast tumors, and (iv) healthy glandular breast tissues using 2D gel electrophoresis, SDS-PAGE, and mass spectrometry in addition to Western blotting. RESULTS: Full-length ezrin (E1; amino acids 1–586) is present in all four investigated tissues. Two truncated ezrin forms, one missing about the first hundred amino acids (E2a) and the other lacking about 150 C-terminal amino acids (E2b) were detectable in primary tumor tissues and in sentinel lymph node metastases but not in glandular tissues. Strikingly, an ezrin truncation (E3) which consists approximately of amino acids 238–586 was found strongly expressed in all sentinel lymph node metastases. Moreover, an N-terminal ezrin fragment (E4) that consists approximately of amino acids 1–273 was identified in sentinel lymph node metastases as well. CONCLUSIONS: We show for the first time the existence of tissue-dependent specific ezrin truncations. The distinguished strong Western blot staining of ezrin E3 in sentinel lymph node metastases underlines its capability to substantiate the occurrence of lymph node (micro)metastases in breast cancer patients.

Translational Oncology (2018) 11, 1–10

Introduction

With about 23% of all new cancer cases worldwide, breast cancer is the most frequent malignant tumor in women. As a result of early detection and improved treatment, breast cancer death rates have been decreasing in North America and in several European countries over the past 25 years [1]. Yet, not the primary tumor but metastases distant from the primary tumor are the reason for approximately 90% of all cancer deaths [2]. Thus, reliable detection of metastases plus adapted follow-up therapy upon primary tumor removal are major clinical challenges today.

Metastatic breast tumor cells preferentially spread through the lymphatic system. Consequently, the initial sites of metastases are in the axillary lymph nodes since they drain the breast tissue in up to 95% of the breast cancer patients and, hence, are the closest downstream neighbors of the primary tumors. The first lymph node(s) draining the primary tumor, the so-called sentinel lymph node(s), are spotted intra-operatively using γ-probes or blue dyes [3].

Addess all correspondence to: Michael O. Glocker, Proteome Center Rostock, University of Rostock, Schillingallee 69, 18057 Rostock, Germany.
E-mail: michael.glocker@med.uni-rostock.de
[1] Both authors contributed equally to this manuscript.
[2] Present address: Praxis für Pathologie Dr. med. D.Rothacker & Kollegen, Ellerried 7, 19,061 Schwerin, Germany.
Received 3 August 2017; Revised 9 October 2017; Accepted 23 October 2017

1936-5233
https://doi.org/10.1016/j.tranon.2017.10.004

Metastases in the sentinel lymph node(s) are found in 20–35% of patients with early-stage breast cancer. The so-called "lymph node status" is an important prognostic factor for further lymph node involvement and patient survival [4,5]. Complete axillary lymph node dissection, though associated with pain, arm swelling, and further complications, had been the traditional operation procedure to both, determine and prevent spreading of the tumor. More recent studies indicated that the sentinel lymph node reflects the downstream nodal status of the corresponding region well, and henceforth sentinel lymph node biopsy has gained comparable prognostic strength, with simultaneously decreased morbidity, since in those cases where occurrence of sentinel lymph node metastases is negative, patients may be spared complete axillary lymph node dissection [3,6–8]. The standard approach for nodal assessment is intraoperative histologic examination of frozen tissue sections of the resected sentinel lymph node [5]. Immuno-histochemical staining of cytokeratin is additionally performed, yet only in cases when hematoxylin and eosin staining gives suspicious, i.e. uncertain indications [9]. Frozen section analysis is a reliable method for the detection of macro-metastases with a sensitivity of up to 92%. However, this method proved to be far less effective (sensitivity of 17%) for the detection of micro-metastases [10,11], requesting improved diagnostic procedures.

Metastasis formation involves several general steps, such as intravasation, circulation, extravasation, and proliferation, but details are still insufficiently understood on both, the cellular and the molecular levels [12]. Ezrin is involved in these processes because it participates in cell adhesion, motility, and cell scattering of degenerated cancer cells as shown by several cell line experiments [13,14]. Ezrin is a member of the ezrin-radixin-moesin (ERM) protein family whose members share approximately 75% sequence homology [15]. Ezrin is composed of three main domains (i) a globular N-terminal domain, the so-called FERM domain, with ~300 amino acids in length, (ii) an alpha helical linker domain (~200 amino acids), and (iii) a positively charged C-terminal domain with ~100 amino acids. Due to the intramolecular binding capability of the C-terminal domain to the FERM domain, ezrin can either form inactive "closed" conformations or homo- and heterodimers with other ERM proteins. In the active ezrin form, the FERM domain — formed by three positively charged lobes, F1-F3 - binds to phosphatidylinositol (4,5)-bisphosphate at the inner layer of the cell membrane upon which threonine residue 567 is phosphorylated. The C-terminal ezrin domain binds to F-actin [16–18]. The most prominent known ezrin function is to form a cross-link between the plasma membrane and cytoskeletal actin fibers (F-actin). Ezrin's N-terminal domain can also bind to several membrane-associated proteins, transmembrane receptors, and co-receptors and, hence, becomes involved in several fundamental signal transduction pathways influencing cell morphology, cell adhesion, cell migration and invasion, proliferation, and survival [16,17,19]. These functional involvements point towards decisive roles of ezrin in metastatic processes of gynecologic cancers [20,21]. Of note, ezrin expression is regulated by estrogen via co-activating proteins [22], highlighting ezrin's importance in breast cancer-related and metastasis-forming processes.

Tissue microarray immunohistochemistry experiments indicate that ezrin is highly over-expressed in breast cancer tissue as compared to control tissue [23]. Moreover, high ezrin expression correlates with occurrence of lymph node metastases and poor patient survival prognosis [24,25]. Interestingly, not only the expression rate but also the cellular localization of ezrin has been found altered in breast cancer cells as opposed to cells from unaffected tissue. While in normal polarized epithelial cells ezrin concentrates at the apical surfaces [26], its localization is shifted to the cytoplasm in most breast cancer cases. Yet, up to now reasons for this change in localization are unknown. To a smaller extent ezrin is found attached to the cell membrane all around the tumor cells [27,28]. High cytoplasmic ezrin staining in tumor cells has been associated with lymph node metastasis occurrence and poor patient survival as well [25,29]. Again, a protein structural explanation of this observation is still lacking.

Our goal was to investigate possible expression differences of ezrin and potential ezrin truncations in sentinel lymph node metastases, in unaffected axillary lymph nodes, in breast tumor tissue, and in healthy glandular breast tissue of breast cancer patients using Western blotting, 2D gel electrophoresis in combination with mass spectrometry, and SDS-PAGE combined with mass spectrometry. Furthermore, we aimed to determine whether structural alterations in ezrin may occur and if so which structural alterations may be found with potential tumor/metastasis-associated cellular localization differences. In fact, we identified tissue-dependent specific patterns of ezrin truncations. A C-terminal ezrin truncation (aa 238–586) was only found strongly expressed in sentinel lymph node metastasis tissues indicating its potential to become a molecular marker by which the presence of lymph node (micro)metastases may be substantiated in breast cancer patients in the future.

Materials and Methods

Human Tissue Samples

Tissues were taken at the Women's University Hospital, Südstadt Clinical Center Rostock, Germany, after informed consent was given from all individual patients included in the study. The study was approved by the Institutional Review board (ethical vote Reg.-No.: A 01/2006 from the Ärztekammer Mecklenburg-Vorpommern). We collected metastases that were prepared from sentinel lymph nodes of 12 women diagnosed with invasive breast cancer of histologic grades two or three and tumor sizes between 15 mm and 35 mm in diameter. We also investigated ten unaffected axillary lymph nodes from two individuals diagnosed with invasive carcinoma of the breast. Additionally, we examined tumors of invasive breast carcinoma and healthy glandular tissues (controls), originating from the same breast, from seven postmenopausal women that underwent modified radical mastectomy. Tumor sizes ranged from 14 mm to 74 mm in diameter and histologic gradings of the tumors were two or three (for patient demographic and clinical data see Supplementary Table 1). All tissues were subjected to routine pathological examination after surgery [30–33]. The tumors, healthy glandular breast tissues, and the axillary lymph nodes were immediately put on ice and transported to the Proteome Center Rostock within 10 minutes. The sentinel lymph nodes were frozen, sliced and stained with hematoxylin/eosin for pathological examination concerning metastasis status. Half of the investigated sentinel lymph node was preserved for preparation of the metastasis tissues. In general, the isolation of the metastasis tissues took no longer than 20 minutes. In the Proteome Center Rostock all tissue pieces were weighed and shock-frozen in liquid nitrogen within 10 minutes and kept at −80 °C until further work-up.

Protein Extract Generation

Protein extract preparation from tissues was conducted as described [34]. Briefly, frozen tissues of approximately 100 mg, each, were ground to powder with a cold pestle in a cold mortar that was kept in a liquid nitrogen bath. The powder was mixed with pre-frozen lysis

buffer (volume [µl]: 9 fold amount of tissue weight in mg) containing 2 M thiourea, 7 M urea, 4% CHAPS, 70 mM Dithiothreitol, 0.5% Servalyte 3–10 (Serva, Heidelberg, Germany), with Complete with EDTA (Roche Diagnostics, Mannheim, Germany) (volume [µl]: 0.4 fold amount of sample weight in mg), and with PMSF/Pepstatin A (Sigma, St. Louis, MO) (volume [µl]: 0.4 fold amount of sample weight in mg). After thawing, glass beads (number = total suspension volume in µl multiplied with 0.034) were added and the suspensions were homogenized by 6 cycles of sonication for 30 sec and stirring on ice for 1 min, respectively. Afterwards, protein extracts were centrifuged for 20 min at 4 °C and 13,000 rpm. Supernatants were aliquoted (100 µl, each), re-frozen in liquid nitrogen and stored at −80 °C for further use. Protein concentrations were determined using the Bio-Rad Protein Assay (Bio-Rad, Munich, Germany) [35,36].

One-Dimensional Gel Electrophoresis

Protein extracts (40 µg total protein, each) were each filled up with de-ionized water to a total volume of 20 µl, mixed with 5 µl sample buffer (312.5 mM Tris–HCl, 10% SDS, 325 mM Dithiothreitol, 50% glycerine, 0.4% bromophenol blue) and heated at 95 °C for 5 min. Protein mixtures were loaded onto a NuPAGE Novex 10% Bis-Tris Gel (Invitrogen, Carlsbad, CA) and SDS-PAGE was carried out in a XCell Sure Lock Mini-Cell (Invitrogen, Carlsbad, CA) with MOPS running buffer (0.05 M MOPS, 0.05 M Tris, 3.46 mM SDS, 0.76% Triplex III) for 50 min applying 200 V constantly. If not used for blotting, proteins in the gels were fixed (50% ethanol, 10% acetic acid) for 1 h and stained with colloidal Coomassie Brilliant Blue G-250 containing aluminum sulfate [37]. The PageRuler Prestained Protein Ladder (Thermo Fisher Scientific, Schwerte, Germany) was used for apparent molecular mass calibration. Stained gels were scanned with the UMAX Mirage II Scanner (Umax Data Systems, Willich, Germany).

Two-Dimensional Gel Electrophoresis

Two-dimensional gel electrophoresis was carried out as described [38]. In short, either protein extracts with 500 µg of protein were loaded onto 18 cm long IEF strips (Immobiline Dry strips, pH 3–10 NL, GE Healthcare Life Sciences, Freiburg, Germany) or protein extracts with 150 µg of protein were loaded onto 7 cm long IEF strips (Immobiline Dry strips, pH 3–10 NL, GE Healthcare Life Sciences). The protein mixtures were mixed with rehydration buffer (8 M urea, 2% CHAPS, 16 mM dithiothreitol, 0.5% IPG buffer (pH 3–10), 4% Complete with EDTA, 1% PMSF/Pepstatin A, and bromophenol blue) to a total volume of 350 µl, and 150 µl, respectively. The first dimension (IEF) was operated in an IPGphor system (GE Healthcare Life Sciences). Strips were equilibrated twice (15 min each) in 5 ml equilibration buffer (50 mM Tris HCl, pH 8.8, 6 M urea, 30% glycerol, 2% SDS, bromophenol blue) supplemented with 1% (w/v) dithiothreitol and 4% (w/v) iodoacetamide, respectively. For the second dimension SDS polyacrylamide gels (12% T) were run for 18 h at 100 V in an Hoefer DALT Vertical Electrophoresis System (GE Healthcare/Amersham Biosciences) or for 1 h at 150 V in a Mini-PROTEAN® 3 Dodeca™ Cell (BIO-RAD), respectively, applying the Laemmli continuous buffer system [39]. Proteins in the gels were fixed and stained with colloidal Coomassie Brillant Blue G-250 [40,41]. Stained gels were scanned with the Umax Mirage II Scanner (Umax Data Systems, Willich, Germany). Images were analyzed using Progenesis PG200, Version 2006 (Nonlinear Dynamics Ltd., Newcastle upon Tyne, UK).

In-Gel Digestion of Proteins and Sample Preparation for Mass Spectrometry

Spots or bands with proteins of interest were excised manually from the 2D- and 1D–SDS gels, respectively, and transferred into an Eppendorf tube. Excised 1D–gel bands were cut into small pieces of approximately 1 mm^3. Gel plugs were washed for 20 min with 30% ACN in 25 mM ammonium bicarbonate (100 µL) and 50% ACN in 10 mM ammonium bicarbonate (100 µL) solutions, respectively. Gels were shrunken after addition of 100 µL ACN and dried afterwards. The dried gel plugs were re-swollen with 5 µL of sequencing grade trypsin solution (Promega, Madison, WI; 9,4 ng/µL in 4,8 mM Tris–HCl, pH 8.5, 5 mM dithiothreitol). In addition, about 3 µl of 3 mM Tris/HCl were added to the1D–gel bands. Digest mixtures were incubated over night at room temperature. Thereafter, 5 µL for 2D–gel spots or 7 µl for 1D–gel bands of extraction solution (0.3% TFA, 50% ACN) were added and the solutions were agitated at room temperature for 60 min. The tryptic peptide mixtures were frozen until further work up. For nanoLC–MS analyses of peptides from 1D–gel bands the supernatant was transferred into a new tube and lyophilized (SpeedVac RVC 2-25CDplus, Martin Christ GmbH, Osterode am Harz, Germany). Lyophylized peptides were dissolved in 10 µl of 3% ACN/0.1% FA by shaking for 20 min. After centrifugation for 2 min at 13000 rpm peptide solutions were diluted 1:10 with 3% ACN/0.1% FA and transferred into 12x32 mm glass neck vials.

MALDI-MS Data Processing

One µl of peptide mixture of digested proteins from 2D–gel spots was mixed with 2 µl DHB matrix (5 mg/ml in ACN/0.1% TFA in water (33/67 v/v)) directly on the target (AnchorChipTM 600/384 target plate, Bruker Daltonik, Bremen, Germany). Peptide mixtures were analyzed with a Reflex III MALDI ToF mass spectrometer (Bruker Daltonik) in positive ion mode [42]. Spectra were externally calibrated using a commercially available Peptide Calibration Standard (Bruker Daltonik) and internally recalibrated using peptide ion signals derived from trypsin autoproteolysis. Mass spectra were further processed and analyzed as previously described [43]. MS/MS spectra were acquired on an Axima MALDI QIT ToF mass spectrometer (Shimadzu Biotech, Manchester, UK) in positive ion mode. Spectra were externally calibrated [44]. About 1000 spectrum profiles were summed and further processing and analysis of the MS/MS spectra was performed with the LaunchpadTM software, version 2.8.4 (Shimadzu Biotech, Manchester, UK).

LC-ESI-MS Configuration

Nanoscale LC separation of tryptic peptides was performed with a nanoACQUITY UPLC system (Waters Corporation, Manchester, UK), equipped with a C18 nanoACQUITY Trap 100 Å 5 µm, 180 µm x 20 mm pre-column (Waters Corporation) and an nanoACQUITY UPLC HSS T3, 10 K psi, 100 Å, 1.8 µm, 75 µm X 150 analytical reversed phase column (Waters Corporation). The peptide mixtures, 2 µl partial loop injection, were initially transferred with an aqueous 0.1% formic acid/0.1% ACN solution to the pre-column at a flow rate of 10 µl/min for 4 min. Mobile phase A was 0.1% formic acid in water whereas mobile phase B was 0.1% formic acid in ACN. After desalting and pre-concentration, the peptides were eluted from the pre-column to the analytical column and separated with a gradient of 3% to 40% mobile phase B within 60 min at a flow rate of 0.3 µl/min, followed by a 13 minute rinse with 85% of mobile phase B. The column was re-equilibrated to achieve initial conditions for 19 min. The column

temperature was maintained at 35 °C. The lock mass compound, [Glu1]-Fibrinopeptide B, was delivered by the auxiliary pump of the LC system at 0.5 µl/min at a concentration of 100 fmol/µl to the reference sprayer of the NanoLockSpray source of the mass spectrometer. The precursor ion masses and associated fragment ion spectra of the tryptic peptides were measured with a SYNAPT G2S HDMS mass spectrometer (Waters Corporation, Manchester, UK) directly coupled to the chromatographic system operated in positive resolution mode. The time-of-flight analyzer of the mass spectrometer was externally calibrated with fragment ions of [Glu1]-Fibrinopeptide B from m/z 50 to 2000, with the data post-acquisition lock mass corrected using the monoisotopic mass of the doubly charged precursor of [Glu1]-Fibrinopeptide B. The reference sprayer was sampled every 60 s. Accurate mass data were collected in data independent mode of acquisition by alternating the energy applied to the collision cell between a low energy and elevated energy state as described previously [45,46]. The alternate scanning method combines peptide MS and multiplexed, data independent peptide fragmentation MS analysis in a single LC–MS experiment for the quantitative and qualitative characterization of a peptide mixture. Briefly, the lock mass corrected spectra are first centroided, de-isotoped, and charge-state-reduced to produce a single accurately measured monoisotopic mass for each peptide and the associated fragment ions. The correlation of a precursor and a potential fragment ion is initially achieved by means of time alignment, followed by a further correlation process during the database search that is based on the physicochemical properties of peptides when they undergo collision induced fragmentation. The spectral acquisition time in each mode was 0.75 s with a 0.015 s inter-scan delay. In low energy MS mode, data were collected at constant trap collision energy of 4 eV and transfer collision energy of 2 eV. In elevated energy MS mode, the trap collision energy maintained 4 eV, while the transfer collision energy was ramped from 20 eV to 45 eV within 0.75 s. One cycle of low and elevated energy data was acquired every 1.5 s.

LC-ESI-MS Data Processing and Protein Identification

LC–MS data were processed using ProteinLynx GlobalSERVER version 2.135.0 (Waters Corporation, Manchester, UK). Protein identifications were obtained by searching a database containing the sequence information of P15311 (Ezrin), P26038 (Moesin), and P35241 (Radixin) obtained from UniProt release 2014_01 - Jan 22, 2014. Search criteria used for protein identification included automatic peptide and fragment ion tolerance settings (approximately 4 and 11 ppm, respectively), 1 allowed missed cleavage, and variable methionine oxidation. Details on the principle of the search algorithm for data independently acquired LC–MS data have been previously presented [47]. Protein identifications were accepted if at least five fragment ions per peptide, ten fragment ions per protein and two peptides per protein were measured. Additionally, each fragment ion spectrum assigned to ezrin was subjected to manual assessment. Fragment ion spectra were excluded when they contained ion signals of poor signal to noise ratios. Spectra that originated from in-source fragmentation were excluded as well.

Western Blot Analysis

Subsequent to gel electrophoretic separation, proteins were electro-blotted onto an Immobilon-FL PVDF transfer membrane (Millipore, Schwalbach, Germany) by semi-dry blotting applying 1.2 mA per cm^2 for 2 h. Membranes were stained 30 seconds in 10 ml of 0.5% (w/v) Ponceau S in 1% acetic acid to control for transfer yield. Blots were then rinsed with 25 ml PBS (Sigma-Aldrich Chemie GmbH, Munich, Germany) and incubated with 10 ml blocking buffer (Odyssey blocking buffer from LI-COR (Lincoln, NE) diluted 1:2 with PBS) for 2 h. Afterwards, blots were probed with the primary antibody (ezrin monoclonal antibody (3C12) from Pierce Biotechnology, Meridian Road Rockford, IL, was used at 0.8 µg/ml and anti-ezrin antibody (EP924Y) from Abcam, Cambridge, UK, was used at dilution 1:1000) in blocking buffer with 0.1% Tween-20 over night at 4 °C. Next, membranes were washed 4 times with 25 ml PBS, 0.1% Tween-20 for 5 min, each, prior to incubation with 10 ml of the secondary antibody solution (IRDye 800 CW goat anti-mouse from LI-COR) diluted 1:15,000 in blocking buffer with 0.1% Tween-20 and 0.02% SDS for 1 h at room temperature. Again, membranes were washed 4 times for 5 min, each, with 25 ml PBS, 0.1% Tween-20. Fluorescence signals were recorded with the Odyssey fluorescence imager (LI-COR) with an excitation wavelength of 800 nm. For representation, the original greyscale images were loaded into CorelDRAW X4 (Corel Corporation, Ottawa, Canada) for manual contrast enhancement using the tone curve function (X:~200, Y:~100). Volumes of the Western blot bands were analyzed using Progenesis PG240 (Nonlinear Dynamics, Newcastle upon Tyne, UK). For each single protein extract, we summed up the volumes of all bands in a given lane and calculated the percentages of these volumes, i.e. of each single ezrin band/form from the total band volumes within a single lane.

Results

Protein Expression Analysis in Lymph Node Metastasis Tissue

Protein extracts from lymph node metastasis tissues from twelve patients were subjected to 2D gel electrophoresis in duplicate, generating a total of 24 2D gels. Typically, 2D gels showed about 1200 well-reproducing protein spots per extract (Figure 1*A*). Among them were the protein spots in which ezrin was identified. Interestingly, mass spectrometric analysis of peptides from picked proteins revealed two ezrin-containing spots in 2D gels of sentinel lymph node metastases at different locations in the gels. One ezrin-containing spot, spot 1, was found at the left of the spot chain in which typically serotransferrin isoforms are identified. This spot located at about 70 kDa and at around pH 6–7, matching with the theoretical molecular masses and pIs of both, ezrin and serotransferrin proteins. Corresponding spots 1 were analyzed from five different gels and the mass spectra of the peptide mixture derived from the protein in these spots (Supplementary Figure 1) showed intense peptide ion signals that were assigned to partial amino acid sequences of ezrin which were distributed all over the complete amino acid sequence, indicating that the full-length ezrin (named E1; aa 1–586) was present in spots 1.

A second ezrin-containing spot, spot 2, was found in the gel regions of about 42 kDa and at pH ~5 where typically cytoplasmic actin 1/2 isoforms are identified. Peptide mapping of the peptide mixture from spots 2 from five different gels revealed that ezrin's N-terminal part was missing (Supplementary Figure 2). The most N-terminal peptide ion signal started at aa 295, indicating that the loss of the N-terminal amino acids (ca. aa 1–294) was responsible for the migration shift to lower apparent masses of this ezrin species (named E3).

The existence of proteotypic peptide ion signals in the analyzed mass spectra confirmed the presence of ezrin or its truncated derivative in both investigated spots and absence of radixin or moesin in these spots since proteotypic peptide ion signals for the latter two

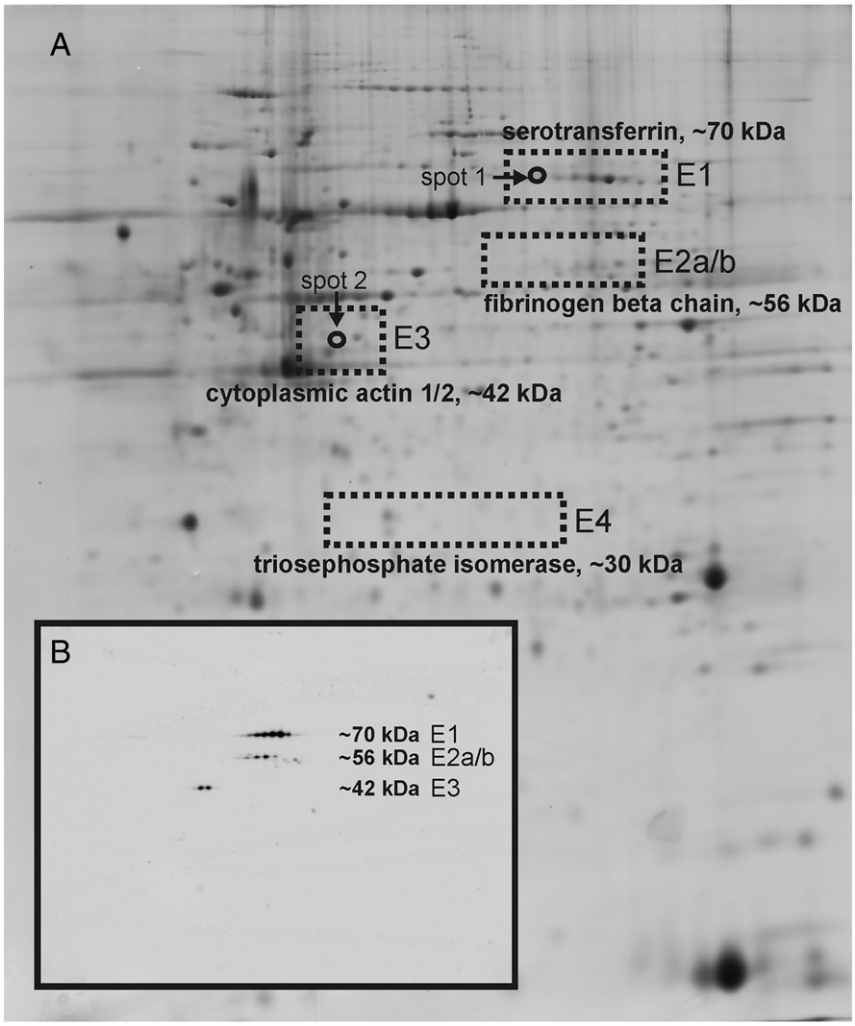

Figure 1. 2D gel analysis of lymph node metastasis tissue proteins and ezrin-specific 2D Western blot.Image of a 2D gel (A) from a protein extract derived from sentinel lymph node metastasis tissue (LNMe J, 500 μg protein, pH 3–10 NL on 18 cm IEF strips, gel: 12% T, Coomassie staining). Four gel regions are framed and the corresponding proteins that typically migrate in these regions are given with their theoretical masses. In spots 1 and 2, ezrin was identified by mass spectrometric peptide mass fingerprinting. Image of a 2D Western blot (B) from a protein extract derived from a sentinel lymph node metastasis (LNMe E, 150 μg, pH 3–10 NL on 7 cm IEF strips, gel: 12% T) after 2DE gel electrophoresis, blotting, and decoration with monoclonal antibody 3C12 which is directed against the C-terminal part of ezrin; epitope region from aa 362 to 585. Approximate masses of the protein spots are given. E1-E4: ezrin forms E1-E4.

proteins were lacking. In order to verify peptide assignments to partial sequences of ezrin, selected peptides, most importantly the proteotypic peptides, were subjected to mass spectrometric fragmentation by which their amino acid sequence assignments were confirmed (data not shown).

Western blot analysis, i.e. decorating ezrin with a monoclonal antibody that is directed against its C-terminal region (3C12: epitope region: aa 362–585), confirmed the presence of ezrin forms E1 and E3 in the two above mentioned spot regions in 2D gels and revealed a third region in between, in which other ezrin-containing spots (named E2) were found (Figure 1*B*). These spots, located at about 55 kDa and pH ~6, overlapped with an area in the 2D gels where typically fibrinogen beta proteins can be identified. Although extensively searching, peptide mass fingerprinting did not identify ezrin or a derivative of ezrin in any of the investigated protein spots of this region. This result may be explained either by too low ezrin abundances in the respective gel area and simultaneous superimposition with other more abundant proteins, or by cross-reactivity of the antibody with other proteins. Interestingly, the antibody staining showed chains of ezrin spots in all three regions, indicating slight structural differences of the ezrin derivatives within each region.

Structure Characterization of Ezrin Truncations in Sentinel Lymph Node Metastases

Since mass spectrometric analysis of 2D gel spots was successful for finding two ezrin derivatives (E1 and E3) in the protein extracts from lymph node metastasis tissues, but was not successful to identify the E2 ezrin form, we analyzed the protein extracts with SDS-PAGE separation in combination with nanoLC-ESI MS^e mass spectrometry. In total, 18 gel bands from protein extracts from sentinel lymph node metastases from several patients were excised and separately examined by mass spectrometry (Figure 2).

Identification of full-length ezrin or truncated ezrin was accepted when at least two peptides were unambiguously assigned to ezrin and

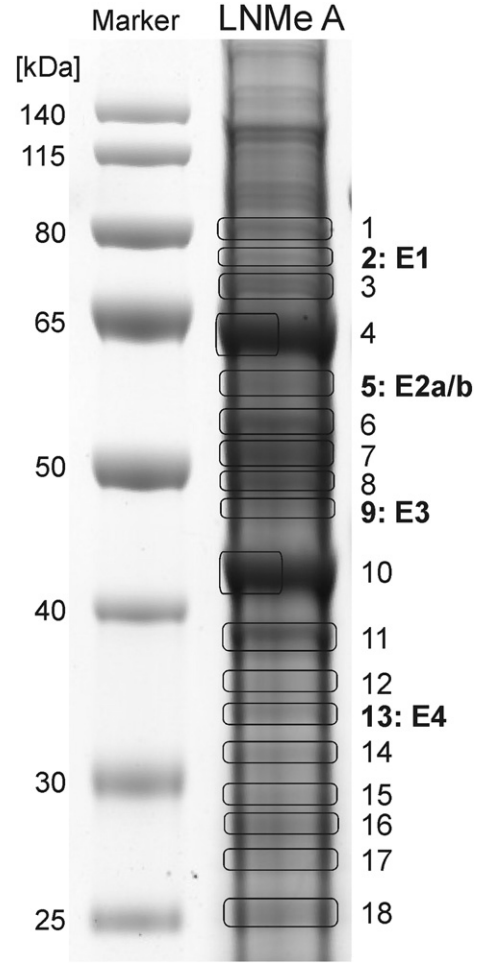

Figure 2. SDS-PAGE of sentinel lymph node metastasis tissue proteins.SDS-PAGE-separated protein extract from sentinel lymph node metastasis tissue (LNMe A, 40 μg protein; gel: 12% T, Coomassie staining). Numbered bands (right) were selected for in-gel digestion and nanoLC-ESI MS^e analysis. Bands in which ezrin species were identified are labeled in bold print. A pre-stained protein ladder was used as apparent molecular mass marker (left). E1-E4: ezrin forms E1-E4.

at least one of them was a proteotypic peptide. Using these criteria, ezrin or its truncations surprisingly were identified in four distinct bands with different apparent molecular masses: (i) band 2 at ca. 75 kDa contained E1, (ii) band 5 at 60 kDa contained E2, (iii) band 9 at about 47 kDa contained E3, and (iv) band 13 at about 33 kDa contained an ezrin form E4.

In-gel digestion experiments were repeated with four more protein extracts of sentinel lymph node metastases from different patients (Supplementary Figure 3, Supplementary Tables 2 and 3) and full-length ezrin (E1) was identified in all five investigated cases with a high number of peptide ions (n = 22–42) in bands 2, many of them (n = 12–24) being proteotypic. Peptide mapping revealed that the identified peptides were distributed over the whole ezrin amino acid sequence. These findings match well with the peptide mapping results from spots 1 in the 2D gels (cf. Figure 1). Thus, it can be concluded that ezrin in band 2 corresponds to ezrin in the serotransferrin region of the 2D gels.

Mass spectrometric analysis of bands 5 identified ezrin in all five investigated lymph node metastasis tissues with 8 to 15 peptides, each; 3 to 7 of them being proteotypic. Analysis of all biological replicates indicated the presence of a C-terminal fragment (E2a), roughly missing the first hundred N-terminal amino acids in four samples (sentinel lymph node metastases (LNMe) of patients B, E, H, and J). The theoretical mass of this form is about 60 kDa (Supplementary Figure 4). Interestingly, LNMe A contained a C-terminally truncated ezrin form, covering amino acids 1–435 with a theoretical mass of about 50 kDa (E2b). Thus, we conclude that ezrin E2 (a and/or b) corresponds to the ezrin derivative that migrates in the fibrinogen beta chain region in the 2D gels/Western blot (cf. Figure 1*B*).

In bands 9 ezrin was identified in three of the five biological replicates with 4 to 9 peptide ions, each; 1 to 3 of them being proteotypic. Peptide mapping clearly indicated the presence of a C-terminal ezrin fragment (E3) covering amino acids 238–586. The theoretical mass of this fragment is about 40 kDa, matching with the findings of the 2D gel spot analysis from spots 2 (cf. Figure 1*A*). Thus, ezrin in bands 9 corresponds to ezrin migrating in the actin region in 2D gels.

Intriguingly, we found an N-terminal fragment of ezrin (E4), covering amino acids 1–273, in bands 13 by mass spectrometric analysis. This form was found in all five biological replicates of the lymph node metastases with 6 to 11 peptides; 1 to 3 of them being proteotypic. Due to its theoretical mass of ~30 kDa and its calculated pI of 5.89 this N-terminal fragment would be expected to migrate in the region of triosephosphate isomerase in the 2D gels (cf. Figure 1*A*). Note, this ezrin fragment was not observed in the immuno-stained 2D gels using the 3C12 antibody because it misses the C-terminal sequence part that carries the epitope region, i.e. the antibody binding site.

In summary, using SDS PAGE in combination with nanoLC-ESI MS^e for protein identification and peptide sequencing of consecutive bands, five ezrin forms (E1, E2a, E2b, E3, and E4) that migrated to four distinct apparent molecular mass ranges by SDS-PAGE were characterized.

Pattern Determination of Distinct Ezrin Truncations in Lymph Node Metastases, Axillary Lymph Nodes, Primary Breast Tumors, and Glandular Breast Tissue

Next, expression of ezrin and its truncations in protein extracts that were generated from different tissues was analyzed by Western blotting after SDS PAGE using the same monoclonal antibody (3C12: epitope region: aa 362–585) as applied above. Investigated protein extracts were from (i) metastases prepared out of sentinel lymph nodes of the axillas from breast cancer patients (sentinel lymph node metastases LNMe, patients A-L, n = 12), and (ii) from unaffected axillary lymph nodes of two breast cancer patients (lymph nodes LN, patients M and N; n = 10), Most interestingly, in the protein extracts from the metastases within the sentinel lymph nodes of breast cancer patients at least three ezrin forms, E1, E2, and E3 were decorated (Figure 3*A*). All protein extracts clearly showed a band corresponding to the full-length protein (E1), whereas six (LNMe A, B, D, E, J, and K) showed a strong band corresponding to ezrin E2 and four (LNMe A, B, D, and E) clearly showed a double band migrating in this region, indicating that in fact two ezrin forms (E2a and E2b) were present. In six protein extracts (LNMe C, F, G, H, I and L) ezrin E2 was expressed in somewhat lower abundance. Yet most importantly, in all twelve sentinel lymph node metastases, ezrin E3 was found strongly stained. Albeit quantification of Western blot bands has a very narrow linear range, we determined the band volume/density of each band within a given lane. Although band intensities of ezrin E3 varied its lowest value in the metastases protein extracts was approx. 10% (Supplementary Table 4).

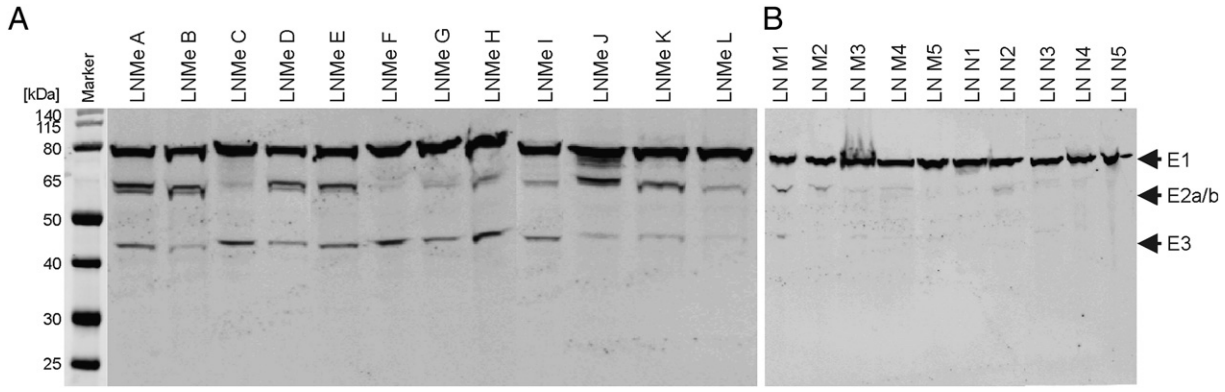

Figure 3. Western blots of ezrin in protein extracts from sentinel lymph node metastases and axillary lymph nodes.Sentinel lymph node metastases (A) of twelve breast cancer patients (LNMe A-L), and unaffected axillary lymph nodes (B) of two breast cancer patients (LN M and N), five each (1–5). Monoclonal anti-ezrin antibody (3C12) with epitope region from aa 362 to 585 was used as primary antibody. A pre-stained protein ladder was used as apparent molecular mass marker (left). E1-E3: ezrin forms E1-E3.

By contrast, all ten unaffected axillary lymph node tissues showed a clear band corresponding to full-length ezrin E1 (Figure 3*B*). In only five of the ten lymph node protein extracts (LN M1 - M4, LN N2) also faintly stained E2 bands were detectable. Strikingly, only one extract from unaffected lymph nodes (LN M1) showed just hints of a band that corresponded to ezrin E3. With strong E3 staining in the metastases it is tempting to speculate that this band indicated presence of (micro)metastases also in this "unaffected" lymph node M1 that may have been overlooked.

Expression of full-length ezrin and its truncations was next analyzed in (i) tissues from invasive breast cancer patients (tumor T, patients O-U, n = 7), and (ii) healthy breast tissues (control/gland G, patients O-U, n = 7) using the 3C12 antibody (epitope region: aa 362–585). In the breast tumors from all seven patients (TO-TU) the full-length ezrin protein (E1) was clearly visible (Figure 4*A*) together with a second band that corresponded to ezrin E2, again found in all seven protein extracts. In three protein extracts (TO, TQ and TS) a third band, possibly corresponding to ezrin E3, was faintly visible. Again, we determined relative band intensities densitometrically; it was obvious that the E2 abundances varied between the tumors (Supplementary Table 5). Ezrin E3, when present, reached again over 10% of the total density in the respective lane.

When analyzing unaffected glandular breast tissues of the same seven patients (GO-GU), we found that exclusively the full-length protein (E1) was expressed in all seven biological replicates, although with lower abundances as compared to those of the tumors (Figure 4*B*). It should be mentioned that it is not possible to compare band intensities from two separate Western blot membranes. Yet, when comparing the percentages of ezrin bands E3 in all extracts, it is obvious, that this form is highly expressed in all the sentinel lymph node metastases extracts and in some of the primary tumor extracts. It is absent in the glandular tissue extracts and has been observed in just one lymph node extract.

Safeguarding of Abundance Pattern Determinations of Ezrin and its Truncations

Ezrin E4 was first characterized by mass spectrometry upon gel electrophoresis, i.e. before proteins were blotted onto membranes. To check for completeness of blotting, we aimed to confirm detection of ezrin E4 in Western blots of selected metastasis protein extracts. As ezrin E4 covers amino acids 1–273, it cannot be decorated by the

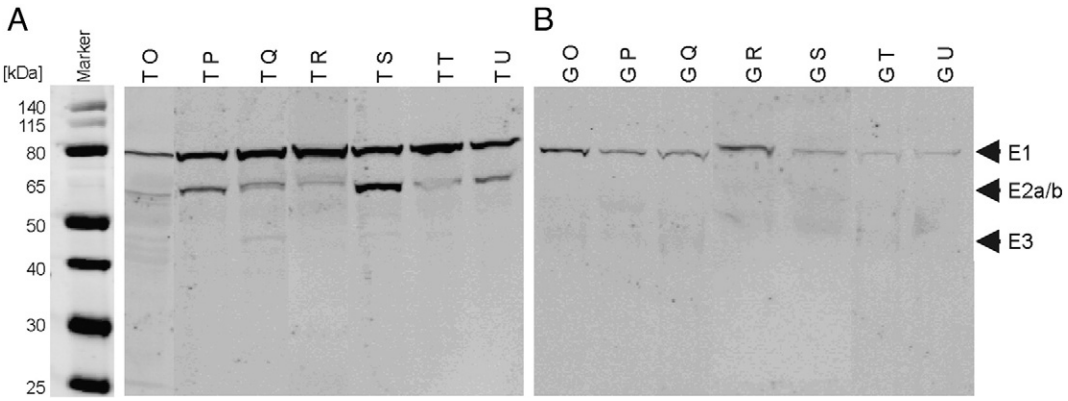

Figure 4. Western blots of ezrin in protein extracts from breast cancer tissues and healthy glandular breast tissues.Primary breast cancer tissues (A) of seven individuals (TO-TU), and healthy glandular breast tissues (B) of the same seven individuals (GO-GU). Monoclonal anti-ezrin antibody (3C12) with epitope region from aa 362 to 585 was used as primary antibody. A pre-stained protein ladder was used as apparent molecular mass marker (left). E1-E3: ezrin forms E1-E3.

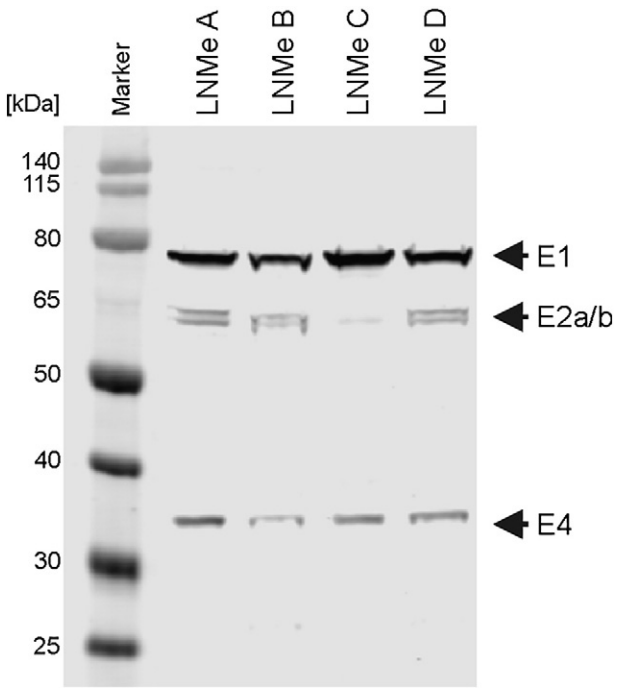

Figure 5. Western blot of ezrin in protein extracts from sentinel lymph node metastases.Sentinel lymph node metastases of four breast cancer patient samples (LNMe A-D) were analyzed using as primary antibody a monoclonal anti-ezrin antibody that targets an epitope around tyrosine residue 145 (EP924Y). A pre-stained protein ladder was used as apparent molecular mass marker (left). E1, E2a/b, and E4: ezrin forms E1, E2a/b, and E4.

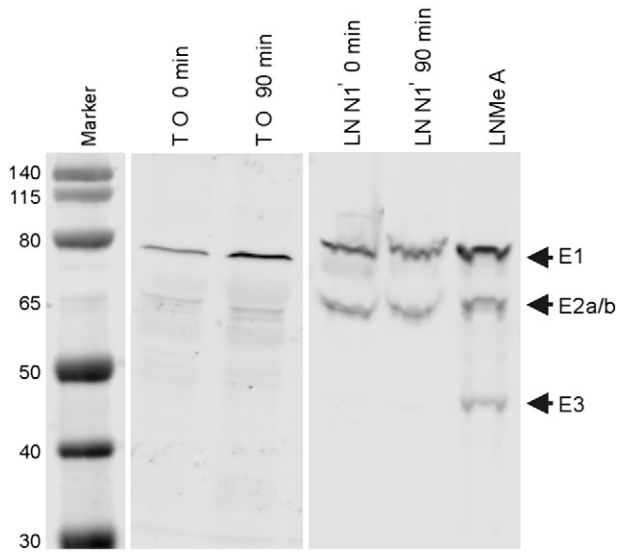

Figure 6. Western blot of ezrin in protein extracts from sentinel lymph node metastases, breast cancer tissues, and axillary lymph nodes.Breast cancer tissue of patient O (TO) and of an unaffected axillary lymph node part of breast cancer patient N (LN N1′). Protein extraction was performed immediately (0 min) after thawing and after keeping the tissues at room temperature for 90 min (90 min). Sentinel lymph node metastasis tissue of patient A (LNMeA) served as control. Monoclonal anti-ezrin antibody (3C12) with epitope region from aa 362 to 585 was used as primary antibody. A pre-stained protein ladder was used as apparent molecular mass marker (left). E1-E3: ezrin forms E1-E3.

3C12 antibody (epitope region: aa 362–585). Thus, we switched to an antibody (EP924Y) that targets the N-terminal part of the protein (epitope around Tyr 145). As expected, Western blotting with sentinel lymph node metastases from four patients A-D (Figure 5) provided clear bands for ezrin E4 at approx. 35 kDa whose relative band intensities were near to 20% (Supplementary Table 6).

In addition, all investigated sentinel lymph node protein extracts showed bands corresponding to the full-length protein (E1). Three extracts (LNMe A, B, and D) showed strong double bands corresponding to ezrin E2. In one protein extract (LNMe C) ezrin E2 was expressed in somewhat lower abundance, consistent with our previous results using the 3C12 antibody. Most importantly, ezrin E3 was not stained. Presence of the ezrin E4 in Western blots confirmed our MS analysis results and showed efficient transfer of all protein bands onto membranes by blotting.

Next, we investigated whether incubation times at room temperature had an effect on ezrin band patterns to exclude that the observed ezrin truncations might have resulted from degradation during sample preparation and transport. Since the different tissues were surgically and pathologically investigated requiring different time durations (see M + M), we divided the tumor from patient O, as well as a piece of the axillary lymph node N1 of patient N (LN N1′) into tissue pieces of approximately same sizes and performed protein extraction either immediately after thawing or after keeping the tissues at room temperature for 90 minutes prior to work-up. Western blotting was performed again and all extracts showed a clear band corresponding to ezrin E1 (Figure 6). A second band, corresponding to ezrin E2, was found in all extracts of both time points as well. Most importantly, no further bands could be detected in the four different tissues, indicating, that the observed ezrin truncations, especially the seemingly metastasis-specific ezrin E3, are not products of rapid proteolytic degradation during sample collection and transport. As control, the protein extract from the sentinel lymph node metastasis of patient A showed three bands (ezrin E1-E3). Of note, the protein extracts of the lymph node tissues and that of the metastasis sample were run on the same gel and, hence, were blotted next to each other.

To confirm that proteins from different tissue extracts, e.g. of metastases, primary tumor, and glandular tissues, result in distinctively different band patterns which were due to *in vivo* processes, we placed some of them next to each other onto one-and-the-same gel and subsequently blotted them as neighboring lanes onto one-and-the-same blot membrane (Supplementary Figure 5).

The aim of this experiment was to exclude that the observed band patterns (see above) were caused by different exposure times, different antibody dilutions, or different transfer conditions between different blots. The appearance of ezrin E3 in only the lanes in which the proteins from the metastasis samples were run proved that the prominent presence of ezrin E3 in the protein extracts of lymph node metastasis tissues was neither caused by unintentional experimental error nor by intentional manipulation.

Summary

Our study shows for the first time a tissue-dependent expression of ezrin truncations. Western blotting using a monoclonal antibody that is directed against ezrin's C-terminal part in combination with mass spectrometric protein structure characterization differentiates four ezrin bands, three of which contain truncations. One truncated ezrin form, E3, lacks approx. 240 amino acids from the N-terminus and

was in our study highly abundant in sentinel lymph node metastases of all 12 breast cancer patients but was – with one exception – absent in 10 unaffected lymph node tissues. E3 was also absent in 7 control tissues, and was only faintly visible in three of seven investigated tumor tissues. With these findings we suggest that ezrin E3 has the potential to serve as metastasis marker in lymph node tissue.

Discussion

Since neither the patients´ genomes nor their tumors´ genomes were sequenced, tumor-specific mutations that result in truncated ezrin proteins cannot be ruled out completely at this time. Alternatively, due to the existence of well-defined ezrin fragments with defined and sharp bands in both, SDS PAGE and Western blot analyses, we assume that specific proteolytic in-vivo cleavages might be made responsible for the observed ezrin truncations. Many cytoskeleton binding proteins, such as ezrin, are known to be substrates of the calcium-dependent proteases of the calpain system [48]. Despite the fact that a consensus sequence for calpain cleavage is not present in ezrin [49] it is a known substrate of this protease family [50–52]. Comparing our findings with literature gives evidence that ezrin E4, containing amino acids 1–273, may be a product of calpain cleavage in the investigated lymph node metastasis tissues. Alternatively, when comparing our results with reports on tissue cultures and animal studies [53–55], caspase-6 might be made responsible for ezrin truncations in the here investigated human lymph node metastases.

To allow ezrin to function as membrane-cytoskeletal linker, the protein has to exhibit two binding sites simultaneously: one at its amino-terminus and one at its carboxy-terminus [19]. We postulate that ezrin truncations that contain only the C-terminus (forms E2a and E3) maintain F-actin binding but cannot adhere to the membrane any more. Due to the missing membrane binding capability these truncated ezrin fragments should be found more abundant in the cytoplasm, which stands in agreement with a strong cytoplasmic ezrin staining in breast tumor tissues [29]. A localization shift to the cytoplasm was also found in locally advanced breast cancer and was associated with positive lymph node status [56]. Changes in the cellular localization of truncated ezrin derivatives in comparison to full-length ezrin have been described in cell culture experiments as well [57]. It is tempting to speculate that accompanying to the structural alterations, ezrin-mediated signaling pathways that stand in context with the metastasis cascade might be affected or even completely interrupted as well.

Conclusion

We have shown that the combination of Western blotting and nanoLC-ESI MS^e after SDS-PAGE as well as 2D gel electrophoresis in combination with mass spectrometric peptide mass fingerprinting was an excellent approach to characterize and to distinguish the pattern of ezrin truncations in the investigated tissues. For the first time we demonstrate that specific ezrin truncations appear in a tissue-dependent manner which adds molecular information to immuno-histological analyses. Based on our investigations we conclude that ezrin E3 has the potential to report the presence of (micro)metastases in sentinel lymph nodes of breast cancer patients. Our mass spectrometry-guided Western blot approach is easy to handle with low-cost laboratory equipment, is highly reproducible, and bears no inter-observer variabilities. Hence, this method may assist the detection of lymph node metastases by the pathologist, and ultimately may improve nodal status determination, and consequently, might allow to give a more precise patient survival prognosis in the future.

Supplementary data to this article can be found online at https://doi.org/10.1016/j.tranon.2017.10.004.

Conflicts of Interest

The authors declare that they have no potential conflicts of interest.

Acknowledgment

We kindly thank M. Ruß, P. Pann, M. Fischer, I. Kacprzyk, F. Henkel, L. John and A. Witt for excellent technical assistance. M. Kreutzer is acknowledged for helpful support concerning the bioinformatic analysis. Funding: The WATERS Synapt G2S mass spectrometer has been bought through an EU grant [EFRE-UHROM 9] made available to MOG.

References

[1] Jemal A, Bray F, Center MMFerlay J, Ward E, and Forman D (2011). Global cancer statistics. *CA Cancer J Clin* **61**, 69–90. https://doi.org/10.3322/caac.20107.

[2] Crnic I and Christofori G (2004). Novel technologies and recent advances in metastasis research. *Int J Dev Biol* **48**, 573–581. https://doi.org/10.1387/ijdb.041809ic.

[3] Luschin G (2010). Sentinel lymph node biopsy in breast cancer. *Wien Med Wochenschr* **160**, 497–500. https://doi.org/10.1007/s10354-010-0830-1.

[4] Chua B, Ung O, Taylor R, and Boyages J (2001). Frequency and predictors of axillary lymph node metastases in invasive breast cancer. *ANZ J Surg* **71**, 723–728. https://doi.org/10.1046/j.1445-1433.2001.02266.x.

[5] Ran S, Volk L, Hall K, and Flister MJ (2010). Lymphangiogenesis and lymphatic metastasis in breast cancer. *Pathophysiology* **17**, 229–251. https://doi.org/10.1016/j.pathophys.2009.11.003.

[6] Albertini J, Lyman G, Cox C, Yeatman T, Balducci L, Ku N, Shivers S, Berman C, Wells K, and Rapaport D, et al (1996). Lymphatic mapping and sentinel node biopsy in the patient with breast cancer. *JAMA* **276**, 1818–1822. https://doi.org/10.1001/jama.1996.03540220042028.

[7] Kühn T, Bembenek A, Buchels H, Decker T, Dunst J, Mullerleile U, Munz DL, Ostertag H, Sautter-Bihl ML, and Schirrmeister H, et al (2004). Sentinel node biopsy in breast cancer. *Nuklearmedizin* **43**, 4–9. https://doi.org/10.1267/NUKL04010004.

[8] Schwartz G, Giuliano A, Veronesi U, and Committee CC (2002). Proceedings of the consensus conference on the role of sentinel lymph node biopsy in carcinoma of the breast April 19 to 22, 2001, Philadelphia, Pennsylvania. *Hum Pathol* **33**, 579–589. https://doi.org/10.1053/hupa.2002.124117.

[9] Seth P, Harlow M, Donald L, and Weaver M (2016). UpToDate, Overview of sentinel lymph node biopsy in breast cancer; 2016.

[10] Wada N, Imoto S, Hasebe T, Ochiai A, Ebihara S, and Moriyama N (2004). Evaluation of intraoperative frozen section diagnosis of sentinel lymph nodes in breast cancer. *Jpn J Clin Oncol* **34**, 113–117.

[11] Weiser MR, Montgomery LL, Susnik B, Tan LK, Borgen PI, and Cody HS (2000). Is routine intraoperative frozen-section examination of sentinel lymph nodes in breast cancer worthwhile? *Ann Surg Oncol* **7**, 651–655.

[12] Leber MF and Efferth T (2009). Molecular principles of cancer invasion and metastasis (review). *Int J Oncol* **34**, 881–895. https://doi.org/10.3892/ijo_00000214.

[13] Elliott BE, Meens JA, SenGupta SK, Louvard D, and Arpin M (2005). The membrane cytoskeletal crosslinker ezrin is required for metastasis of breast carcinoma cells. *Breast Cancer Res* **7**, R365-73. https://doi.org/10.1186/bcr1006.

[14] Elliott BE, Qiao H, Louvard D, and Arpin M (2004). Co-operative effect of c-Src and ezrin in deregulation of cell-cell contacts and scattering of mammary carcinoma cells. *J Cell Biochem* **92**, 16–28. https://doi.org/10.1002/jcb.20033.

[15] Sato N, Funayama N, Nagafuchi A, Yonemura S, and Tsukita S (1992). A gene family consisting of ezrin, radixin and moesin. Its specific localization at actin filament/plasma membrane association sites. *J Cell Sci* **103**(Pt 1), 131–143.

[16] Clucas J and Valderrama F (2014). ERM proteins in cancer progression. *J Cell Sci* **127**, 267–275. https://doi.org/10.1242/jcs.133108.

[17] Fehon RG, McClatchey AI, and Bretscher A (2010). Organizing the cell cortex: the role of ERM proteins. *Nat Rev Mol Cell Biol* **11**, 276–287. https://doi.org/10.1038/nrm2866.

[18] Gary R and Bretscher A (1995). Ezrin self-association involves binding of an N-terminal domain to a normally masked C-terminal domain that includes the F-actin binding site. *Mol Biol Cell* **6**, 1061–1075. https://doi.org/10.1091/mbc.6.8.1061.

[19] Arpin M, Chirivino D, Naba A, and Zwaenepoel I (2011). Emerging role for ERM proteins in cell adhesion and migration. *Cell Adhes Migr* **5**, 199–206. https://doi.org/10.4161/cam.5.2.15081.

[20] Choi S and Kim T (2012). Ezrin and metastatic behavior of common estrogen dependent tumors. *WebmedCentral Oncol* **3**, 1–18.

[21] Choi S (2012). Ezrin is an essential marker for metastasis of gynecologic cancer. *J Korean Soc Menopause* **18**, 81–93.

[22] Smith PM, Cowan A, Milgram SL, and White BA (2003). Tissue-specific regulation by estrogen of ezrin and ezrin/radixin/moesin-binding protein 50. *Endocrine* **22**, 119–126. https://doi.org/10.1385/ENDO:22:2:119.

[23] Bruce B, Khanna G, Ren L, Landberg G, Jirstrom K, Powell C, Borczuk A, Keller ET, Wojno KJ, and Meltzer P, et al (2007). Expression of the cytoskeleton linker protein ezrin in human cancers. *Clin Exp Metastasis* **24**, 69–78. https://doi.org/10.1007/s10585-006-9050-x.

[24] Li Q, Wu MF, Song AP, Wei JC, Xu G, Lu YP, and Ma D (2006). Expression of Ezrin and E-cadherin in invasive ductal breast cancer and their correlations to lymphatic metastasis. *Ai Zheng* **25**, 363–366.

[25] Yu Z, Sun M, Jin F, Xiao Q, He M, Wu H, Ren J, Zhao L, Zhao H, and Yao W, et al (2015). Combined expression of ezrin and E-cadherin is associated with lymph node metastasis and poor prognosis in breast cancer. *Oncol Rep* **34**, 165–174. https://doi.org/10.3892/or.2015.3967.

[26] Berryman M, Franck Z, and Bretscher A (1993). Ezrin Is Concentrated in the Apical Microvilli of a Wide Variety of Epithelial-Cells Whereas Moesin Is Found Primarily in Endothelial-Cells. *J Cell Sci* **105**, 1025–1043.

[27] Jais MH, Md Zin RR, Muhd Hanapi NA, and Md Ali SA (2015). Ezrin is Significantly Overexpressed in Luminal A, Luminal B, and HER2 Subtype Breast Cancer. *Appl Immunohistochem Mol Morphol* . https://doi.org/10.1097/PAI.0000000000000258.

[28] Li Q, Wu M, Wang H, Xu G, Zhu T, Zhang Y, Liu P, Song A, Gang C, and Han Z, et al (2008). Ezrin silencing by small hairpin RNA reverses metastatic behaviors of human breast cancer cells. *Cancer Lett* **261**, 55–63. https://doi.org/10.1016/j.canlet.2007.11.018.

[29] Sarrio D, Rodriguez-Pinilla SM, Dotor A, Calero F, Hardisson D, and Palacios J (2006). Abnormal ezrin localization is associated with clinicopathological features in invasive breast carcinomas. *Breast Cancer Res Treat* **98**, 71–79. https://doi.org/10.1007/s10549-005-9133-4.

[30] Elston CW (2005). Classification and grading of invasive breast carcinoma. *Verh Dtsch Ges Pathol* **89**, 35–44.

[31] Kleihues P and Sobin LH (2003). Pathology and Genetics of Tumours of the Breast and Female Genital Organs. International Agency for Research on Cancer (IARC). Lyon: World Health Organization Classification of Tumours; 2003.

[32] Perry N, Broeders M, de Wolf C, Törnberg S, Holland R, and von Karsa L (2006). European guidelines for quality assurance in breast cancer screening and diagnosis. Luxembourg: Office for Official Publications of the European Communities; 2006 .

[33] Remmele W and Stegner HE (1987). Recommendation for uniform definition of an immunoreactive score (IRS) for immunohistochemical estrogen receptor detection (ER-ICA) in breast cancer tissue. *Pathologe* **8**, 138–140.

[34] Just T, Gafumbegete E, Gramberg J, Prüfer I, Mikkat S, Ringel B, Pau HW, and Glocker MO (2006). Differential proteome analysis of tonsils from children with chronic tonsillitis or with hyperplasia reveals disease-associated protein expression differences. *Anal Bioanal Chem* **384**, 1134–1144. https://doi.org/10.1007/s00216-005-0288-y.

[35] Bradford MM (1976). A rapid and sensitive method for the quantitation of microgram quantities of protein utilizing the principle of protein-dye binding. *Anal Biochem* **72**, 248–254.

[36] Lorenz P, Bantscheff M, Ibrahim SM, Thiesen H-J, and Glocker MO (2003). Proteome analysis of diseased joints from mice suffering from collagen-induced arthritis. *Clin Chem Lab Med* **41**, 1622–1632.

[37] Kang D, Gho YS, Suh M, and Kang C (2002). Highly Sensitive and Fast Protein Detection with Coomassie Brilliant Blue in Sodium Dodecyl Sulfate-Polyacrylamide Gel Electrophoresis. *Bull Kor Chem Soc* **23**, 1511–1512. https://doi.org/10.5012/bkcs.2002.23.11.1511.

[38] Sinz A, Bantscheff M, Mikkat S, Ringel B, Drynda S, Kekow J, Thiesen H-J, and Glocker MO (2002). Mass spectrometric proteome analyses of synovial fluids and plasmas from patients suffering from rheumatoid arthritis and comparison to reactive arthritis or osteoarthritis. *Electrophoresis* **23**, 3445–3456. https://doi.org/10.1002/1522-2683(200210)23:19<3445::AID-ELPS3445>3.0.CO;2-J.

[39] Laemmli UK (1970). Cleavage of structural proteins during the assembly of the head of bacteriophage T4. *Nature* **227**, 680–685. https://doi.org/10.1038/227680a0.

[40] Bantscheff M, Ringel B, Madi A, Schnabel R, Glocker MO, and Thiesen H-J (2004). Differential proteome analysis and mass spectrometric characterization of germ line development-related proteins of Caenorhabditis elegans. *Proteomics* **4**, 2283–2295.

[41] Neuhoff V, Arold N, Taube D, and Ehrhardt W (1988). Improved staining of proteins in polyacrylamide gels including isoelectric focusing gels with clear background at nanogram sensitivity using Coomassie Brilliant Blue G-250 and R-250. *Electrophoresis* **9**, 255–262. https://doi.org/10.1002/elps.1150090603.

[42] Mikkat S, Koy C, Ulbrich M, Ringel B, and Glocker MO (2004). Mass spectrometric protein structure characterization reveals cause of migration differences of haptoglobin a chains in two-dimensional gel electrophoresis. *Proteomics* **4**, 3921–3932. https://doi.org/10.1002/pmic.200400825.

[43] Röwer C, Koy C, Hecker M, Reimer T, Gerber B, Thiesen HJ, and Glocker MO (2011). Mass spectrometric characterization of protein structure details refines the proteome signature for invasive ductal breast carcinoma. *J Am Soc Mass Spectrom* **22**, 440–456. https://doi.org/10.1007/s13361-010-0031-6.

[44] Koy C, Mikkat S, Raptakis E, Sutton C, Resch M, Tanaka K, and Glocker MO (2003). Matrix-assisted laser desorption/ionization-quadrupole ion trap-time of flight mass spectrometry sequencing resolves structures of unidentified peptides obtained by in-gel tryptic digestion of haptoglobin derivatives from human plasma proteomes. *Proteomics* **3**, 851–858. https://doi.org/10.1002/pmic.200300381.

[45] Silva JC, Denny R, Dorschel CA, Gorenstein MV, Kass IJ, Li G-Z, McKenna T, Nold MJ, Richardson K, and Young P, et al (2005). Quantitative Proteomic Analysis by Accurate Mass Retention Time Pairs. *Anal Chem* **77**, 2187–2200. https://doi.org/10.1021/ac048455k.

[46] Geromanos SJ, Silva JC, Vissers JPC, Dorschel CA, Li G-Z, Gorenstein MV, Bateman RH, and Langridge JI (2009). The detection, correlation and comparison of peptide precursor and products ions from data independent LC-MS with data dependant LC-MS/MS. *Proteomics* **9**, 1683–1695. https://doi.org/10.1002/pmic.200800562.

[47] Li G-Z, Vissers JPC, Silva JC, Golick D, Gorenstein MV, and Geromanos SJ (2009). Database Searching and Accounting of Data Independent Acquired Precursor and Products Ions from Simple and Complex Peptide Mixtures. *Proteomics* **9**, 1696–1719. https://doi.org/10.1002/pmic.200800564.

[48] Franco SJ and Huttenlocher A (2005). Regulating cell migration: calpains make the cut. *J Cell Sci* **118**, 3829–3838. https://doi.org/10.1242/jcs.02562.

[49] Tompa P, Buzder-Lantos P, Tantos A, Farkas A, Szilagyi A, Banoczi Z, Hudecz F, and Friedrich P (2004). On the sequential determinants of calpain cleavage. *J Biol Chem* **279**, 20775–20785. https://doi.org/10.1074/jbc.M313873200.

[50] Kaul SC, Kawai R, Nomura H, Mitsui Y, Reddel RR, and Wadhwa R (1999). Identification of a 55-kDa ezrin-related protein that induces cytoskeletal changes and localizes to the nucleolus. *Exp Cell Res* **250**, 51–61. https://doi.org/10.1006/excr.1999.4491.

[51] McRobert EA, Young AN, and Bach LA (2012). Advanced glycation end-products induce calpain-mediated degradation of ezrin. *FEBS J* **279**, 3240–3250. https://doi.org/10.1111/j.1742-4658.2012.08710.x.

[52] Yao X, Thibodeau A, and Forte JG (1993). Ezrin-calpain I interactions in gastric parietal cells. *Am J Phys* **265**, C36–46.

[53] Cho JH, Lee PY, Son WC, Chi SW, Park BC, Kim JH, and Park SG (2013). Identification of the novel substrates for caspase-6 in apoptosis using proteomic approaches. *BMB Rep* **46**, 588–593. https://doi.org/10.5483/BMBRep.2013.46.12.081.

[54] Klaiman G, Petzke TL, Hammond J, and Leblanc AC (2008). Targets of caspase-6 activity in human neurons and Alzheimer disease. *Mol Cell Proteomics* **7**, 1541–1555. https://doi.org/10.1074/mcp.M800007-MCP200.

[55] Nicholson DW (1999). Caspase structure, proteolytic substrates, and function during apoptotic cell death. *Cell Death Differ* **6**, 1028–1042. https://doi.org/10.1038/sj.cdd.4400598.

[56] Arslan AA, Silvera D, Arju R, Giashuddin S, Belitskaya-Levy I, Formenti SC, and Schneider RJ (2012). Atypical ezrin localization as a marker of locally advanced breast cancer. *Breast Cancer Res Treat* **134**, 981–988. https://doi.org/10.1007/s10549-012-2017-5.

[57] Crepaldi T, Gautreau A, Comoglio PM, Louvard D, and Arpin M (1997). Ezrin is an effector of hepatocyte growth factor-mediated migration and morphogenesis in epithelial cells. *J Cell Biol* **138**, 423–434.